

ELECTRONIC BAND STRUCTURES OF THE SCHEELITE TUNGSTATES AND CONSEQUENCES FOR MATERIAL PROPERTIES

N. A. W. Holzwarth, Yaochun Zhang, and Richard Williams

Wake Forest University, Winston-Salem, NC. USA

We report the results of electronic structure calculations for CaWO_4 and PbWO_4 in the scheelite structure and of a hypothetical mixed CaWO_4 - PbWO_4 crystal. The results give a variational approximation to the ground-state electron densities of these materials within the framework of density functional theory and help us formulate a qualitative understanding of the bonding mechanisms. In addition, we report an approximate analysis of the optical dielectric constants and reflectivity of CaWO_4 and PbWO_4 .

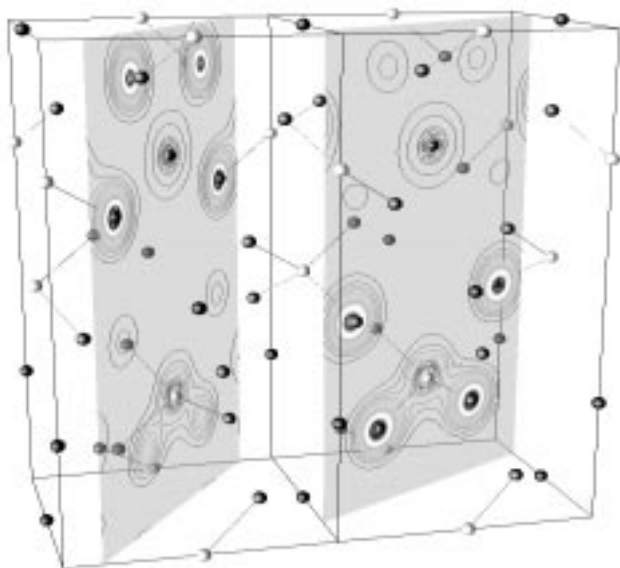


Figure 1: Perspective drawing of two conventional unit cells of PbWO_4 . The atomic positions are indicated with spheres. Lines indicate the approximately tetrahedral W-O bonds. Two different planes, both passing through Pb and W sites are also shown. The left plane passes through two O sites which are nearest neighbors of Pb in approximately octahedral coordination. The right plane passes through two tetrahedral W-O bonds. Contour plots of the electron valence density are plotted in the planes.

Introduction

While the scheelite tungstate crystals have been studied for many years, some very basic questions about the bonding mechanisms in the perfect crystals and in defects are still unknown. Traditional density functional methods [1, 2] can help us to

understand the ground electronic states and can provide an approximate framework for discussing features of the optical properties for these materials. We have recently published[3] a study of the four related scheelite materials – CaMoO_4 , CaWO_4 , PbMoO_4 , and PbWO_4 . In the present paper, we summarize some of those results and also present results for a mixed crystal which crudely approximates the effects of Pb impurities in a CaWO_4 crystal. In addition, we present results for the imaginary part of the dielectric constant calculated using the Kohn-Sham wavefunctions and eigenvalues as a zeroth order approximation to the optical excitation processes in these crystals.

Calculational methods

The calculations reported in this paper were performed with the LAPW technique using the **WIEN97**[4] code. The exchange-correlation functional was taken within the local density approximation using the form developed by Perdew and Wang[5]. The calculational and convergence parameters used in these calculations were the same as those detailed in our previous paper [3] except for the \mathbf{k} -point sampling. In the previous work, the Brillouin zone integration of the self-consistent electron density was approximated within the tetrahedron method[6] using 6 irreducible \mathbf{k} -points corresponding to 27 \mathbf{k} -points throughout the Brillouin zone. For the mixed crystal which has lower symmetry, we needed to use 8 irreducible \mathbf{k} -points to achieve the same accuracy. For the calculation of the optical properties, the results are much more sensitive to the \mathbf{k} -point sampling than is the self-consistent ground-state electron density. Therefore, we used 35 irreducible \mathbf{k} -points corresponding to 216 \mathbf{k} -points throughout the Brillouin zone for calculating the imaginary part of the dielectric constant.

Ground-state properties of pure crystals of Ca and Pb tungstate

Figure 1 shows a perspective drawing of two conventional unit cells of PbWO_4 and contour plots of the valence electron density. The corresponding plots for CaWO_4 looks very similar except that there is much less valence charge around the Ca site compared to the density about the Pb state due to the Pb 6s states shown in Fig. 1. The main contributions to the electron density seen in this figure are due to charge in the vicinity of the oxygen sites. In this plot, covalent bonding between the O and W sites is clearly evident, while it is not obvious that there is appreciable covalent bonding between the O and Pb sites. If one considers the extent of the Pb 6s wavefunction in the context of the crystal geometry, it is clear that there is

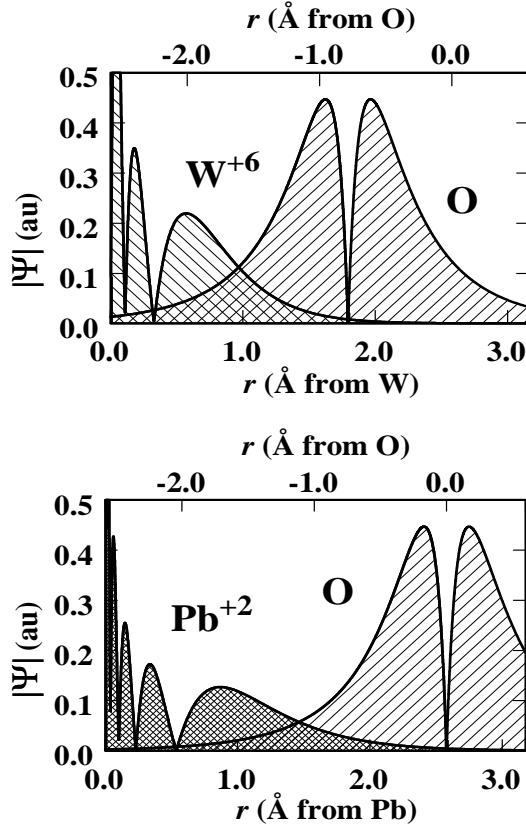


Figure 2: Atomic and ionic wavefunction magnitudes are plotted along nearest neighbor Pb – O and W – O directions in the geometry of a PbWO_4 crystal.

appreciable overlap of this state with its neighbors in the crystal. Fig. 2 shows the overlap of the ionic $6s$ wavefunction of Pb^{+2} with an atomic $2p$ wavefunction of O at its nearest neighbor site in the crystal in comparison with a similar plot for the ionic $5d$ wavefunction of W^{+6} . This plot suggests that the Pb could have some covalent behavior in these compounds.

Figure 3 shows the valence band partial densities of states for CaWO_4 and PbWO_4 . The plots presented here were based on the 35 \mathbf{k} -point sampling of the Brillouin zone and therefore differ slightly from the results presented in our earlier work. The two plots look very similar except that PbWO_4 has a very narrow band below the main valence band which is largely due to the Pb $6s$ states and CaWO_4 has a substantial contribution from the unbound Ca $3d$ excited states above the conduction band, as noted in our previous work. From this partial density of states plot and further analysis in our earlier work, is apparent that states in the vicinity of the band gap are well described by the molecular orbital picture developed by Ballhausen[7] for the WO_4^{-2} complex. The lower part of the valence band has states of mostly O $2p\sigma$ character hybridized with W $5d$ states, while the upper part has

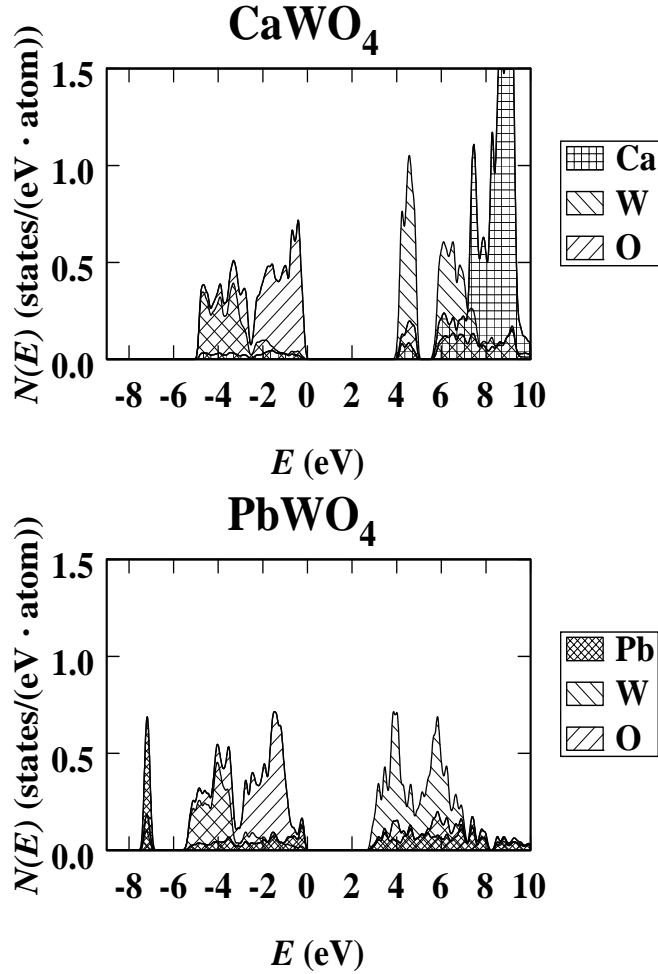


Figure 3: Partial densities of states are plotted for CaWO_4 and PbWO_4 . The weight factors for the partial densities of states are taken as the charge within each muffin tin sphere for each state. In this figure and throughout this paper, the zero of energy is adjusted to be the energy of the last occupied state.

mostly states of O $2p\pi$ character. The bottom of the conduction band is dominated by states of W $5d$ character and the crystal field causes the splitting of the lower states of e symmetry from the upper states of t_2 symmetry. On this scale, Pb states apparently play a very minor role in the valence band structure of PbWO_4 . However, as we shall see below, this first impression is not the entire story.

Results for the band dispersions for these materials are reproduced in figure 4. Here we see that CaWO_4 has band extrema at the Γ point, while PbWO_4 has a more complicated dispersion.

Mixed crystal of Ca and Pb tungstate

Pb impurities introduced into CaWO_4 single crystals were studied with detailed EPR measurements by Born, Hofstaetter, and Scharmann [8, 9, 10, 11] in the 1970's.

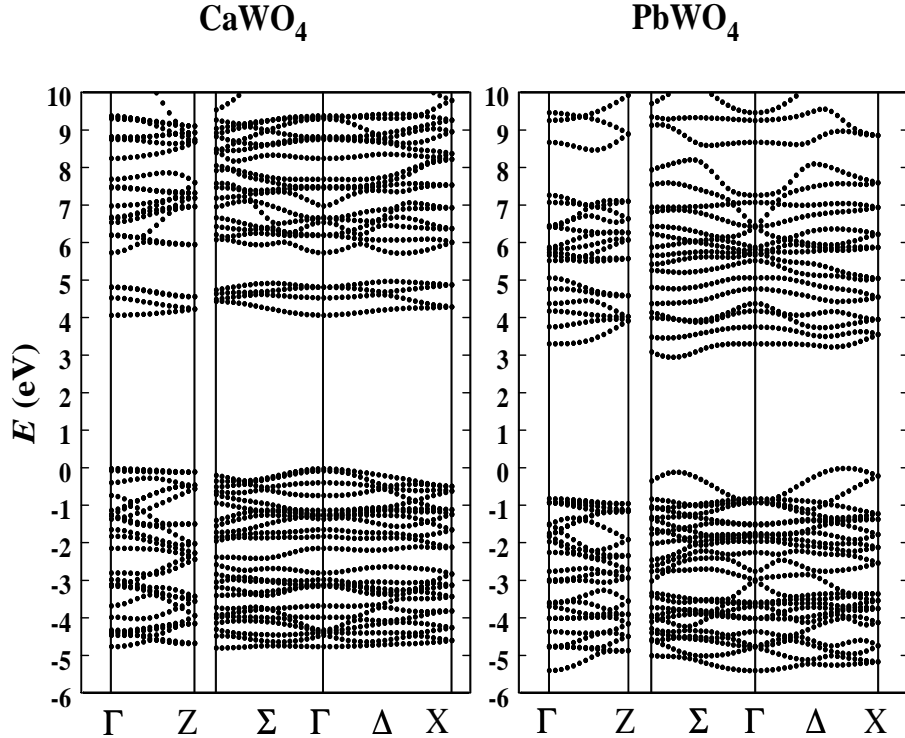


Figure 4: The band structure diagrams for pure CaWO_4 and PbWO_4 , are plotted using the Brillouin zone labels defined in Ref. [3].

This work clearly identified the presence of an impurity state within the band gap having appreciable density associated with a Pb $6s$ state. In order to investigate this system with the same techniques used to study the pure materials, we carried out a simulation for a mixed crystal based on a perfect CaWO_4 lattice described by the experimental lattice parameters [12], replacing every other Ca site with Pb. The idea was to perform a super cell calculation to approximate the impurity system. Obviously, a mixed crystal with 50% CaWO_4 and 50% PbWO_4 is a rather gross approximation for the dilute impurity system studied experimentally. However, we expect that our simulation system can give us important qualitative information.

Results for the partial density of states for the mixed crystal are presented in Fig. 5. This result looks very much like a superposition of the two curves shown in Fig. (2) for the pure crystals, except for the appearance of some distinctive peaks in the partial density of states for states of primarily Pb character in what would correspond to the band gap. In order to investigate this further we have made contour plots for the electron density associated with these states. These are presented in Fig. 6, together the corresponding plot for the sub-valence band state also associated with the Pb $6s$ states. From these plots, especially within the

**Partial density of states
for mixed CaWO_4 - PbWO_4 crystal**

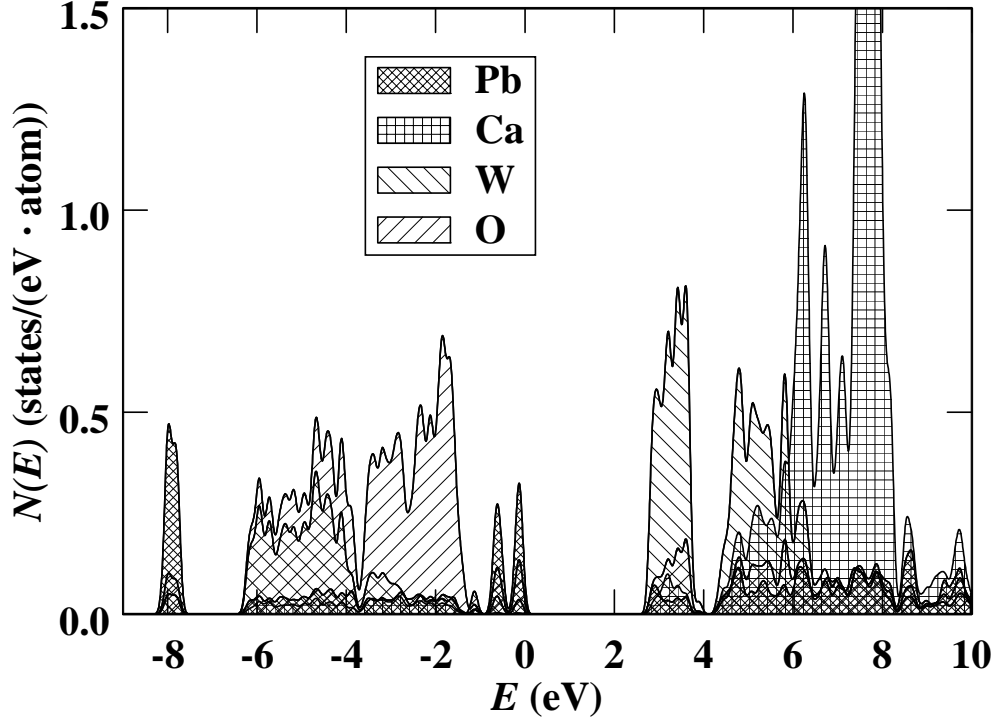


Figure 5: The partial density of states for hypothetical mixed crystal of CaWO_4 and PbWO_4 are plotted using weight factors based on the charge within each sphere for each state.

plane that passes through the Pb sites and the nearest neighbor O sites, one can see clear evidence of covalent bonding. For the lower state there is a build up of charge between the Pb and O sites, indicating a bonding molecular orbital. For the upper state, there is no charge between the Pb and O sites, indicating an *anti-bonding* molecular orbital.

On the basis of the mixed crystal results, one might wonder whether there is similar covalent bonding in pure PbWO_4 . We constructed contour plots similar to those shown in Fig. 6 for PbWO_4 , and did find very similar results. This suggests that in PbWO_4 , a bonding combination of Pb 6s and O 2p states contributes to the sub-valence band state, while an antibonding combination of those states contribute throughout the conduction band, but especially at the top of the valence band.

Optical properties

Calculation of optical properties of materials is beyond the scope of density functional theory which is rigorously a ground-state formalism. However, there has

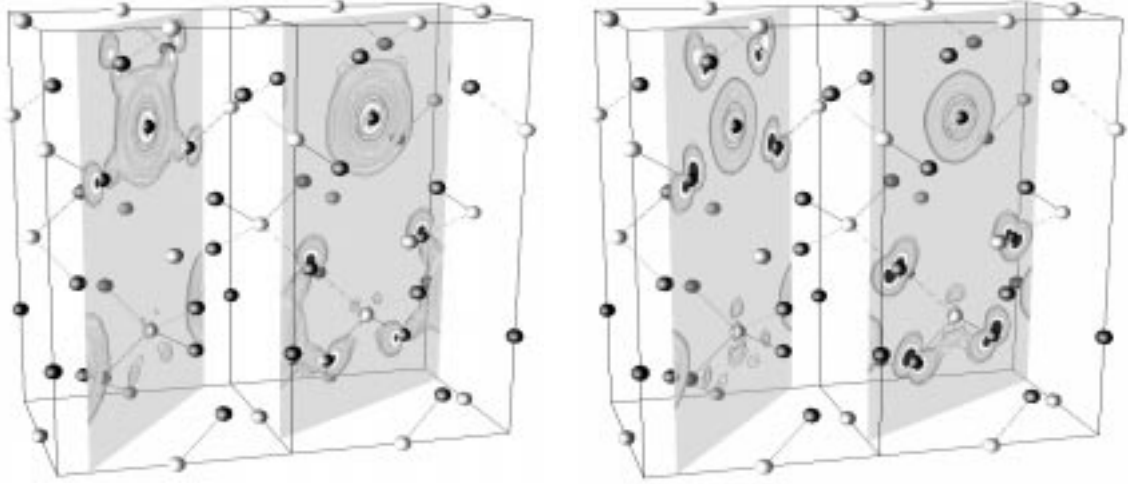


Figure 6: Perspective contour diagram (similar to Fig. (1)) of selected charge density for the mixed crystal, comparing subvalence band states (left) and band gap states (right). Since this density corresponds to only 2 electrons per unit cell, the contour levels shown correspond to $1/200^{\text{th}}$ of the density shown in Fig. (1).

recently been considerable progress in developing methods to calculate optical properties using density functions as the starting point [13, 14]. As a first step toward investigating the optical properties, we have calculated the imaginary part of the dielectric constant using the self-consistent LAPW wavefunctions $\Psi_{n\mathbf{k}}(\mathbf{r})$ and one-electron eigenvalues $E_{n\mathbf{k}}$, using the code developed by Abt and Ambrosch-Draxl [15]. The imaginary part of the dielectric constant corresponding to the electric field polarized in the direction α is can be estimated from the sum of matrix elements:

$$\begin{aligned}
 \text{Im}(\epsilon_{\alpha\alpha}(h\nu)) = & \quad (1) \\
 \frac{4\pi\hbar^2 e^2}{m^2(h\nu)^2} \sum_{n_i n_f} \int \frac{2d^3k}{(2\pi)^3} & \quad |\langle \Psi_{n_i\mathbf{k}} | p_\alpha | \Psi_{n_f\mathbf{k}} \rangle|^2 f_{n_i\mathbf{k}}(1 - f_{n_f\mathbf{k}})\delta(E_{n_f\mathbf{k}} - E_{n_i\mathbf{k}} - h\nu),
 \end{aligned}$$

where the indices n_i and n_f refer to the initial and final state bands, $f_{n\mathbf{k}}$ denotes the Fermi factor, and p_α denotes the momentum operator. Equation 2 was evaluated for a 30 eV range of initial and final states represented by the LAPW wavefunctions. The Brillouin zone integration was approximated by using the tetrahedron method at 35 \mathbf{k} -points within the irreducible section of the Brillouin zone. We checked the convergence of the Brillouin zone integration and found that the main features of the results could be reproduced with a smaller number of \mathbf{k} -points.

The results for CaWO_4 and PbWO_4 are presented in Fig. 7. For both materials, there is a significant difference between the detailed form of $\text{Im}(\epsilon_{\alpha\alpha})$ for the electric field polarized along the a- or c- axes. The main oscillator strength shown in these results corresponds to transitions between states associated with the WO_4 complex.

For CaWO_4 , there is a contribution at $h\nu \approx 27\text{eV}$ associated with transitions between the Ca $3p$ core states and the Ca $3d$ resonant states. Additional analysis is needed to identify some of the other features of the calculated spectrum.

For PbWO_4 , one interesting feature of these results is a sharp contribution at the absorption threshold. This feature is due to an approximate singularity in the joint density of states in this energy region. In figure 4, it is apparent that the valence band and conduction band extrema along the Σ and Δ directions of the Brillouin zone could contribute to this feature. It is also amusing to note that this feature is much larger when the electric field is polarized along the a-axis than it is when the field is polarized along the c-axis. In order to further investigate the states involved with this distinctive feature in the dielectric constant, we constructed a contour plot for the charge density associated with the states near the top of the valence band in PbWO_4 . The results looked similar to the mixed crystal result shown in the right diagram of Fig. 6, clearly indicating that the initial states of these transitions are anti-bonding combinations of Pb $6s$ and O $2p$ states.

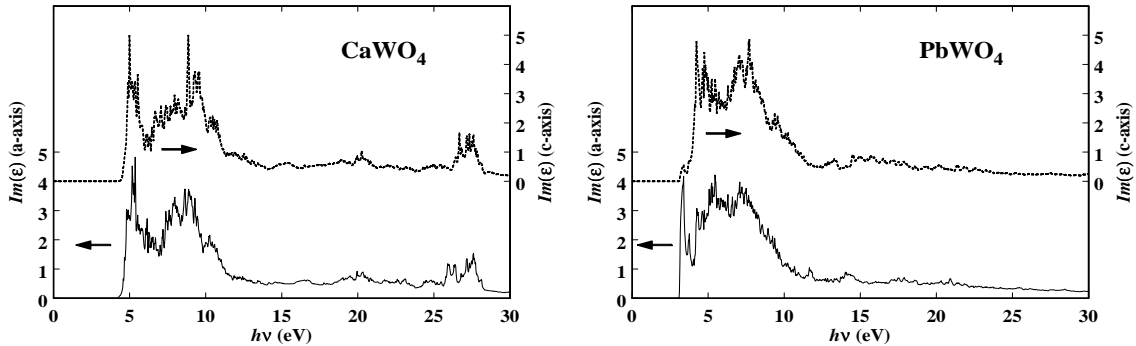


Figure 7: Values of the imaginary part of the dielectric constant of CaWO_4 and PbWO_4 calculated from the LAPW wavefunctions over a 30 eV range of photon energies $h\nu$ showing results for an electric field polarized along an a-axis and for an electric field polarized along the c-axis as indicated.

In order to compare these results with experiment, we calculated the corresponding reflectivity associated normal incidence, considering a-axis and c-axis polarizations separately. In order to calculate the reflectivity, we must first calculate the real part of the dielectric constant by evaluating the Kramers-Kronig transform of Eq. 2. Since, we have only evaluated $Im(\epsilon_{\alpha\alpha})$ within a 30 eV range of energy, there will be some truncation error involved. We present the uncorrected reflectivities calculated for CaWO_4 and PbWO_4 in Fig. 8.

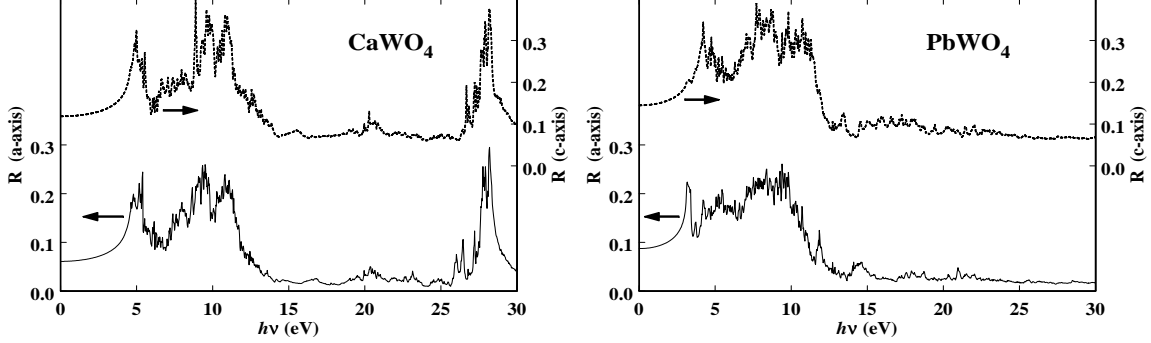


Figure 8: Values of the reflectivity of CaWO_4 and PbWO_4 calculated from the LAPW wavefunctions over a 30 eV range of photon energies $h\nu$ showing results for an electric field polarized along an a-axis and for an electric field polarized along the c-axis as indicated. The values of $Re(\epsilon_{\alpha\alpha})$ used for this plot were determined by using a Kramers-Kronig transform which were not corrected for contributions from higher energy transitions.

In order to estimate the error in the truncation of the Kramers-Kronig integral, we first evaluated the f -sum rule within the 30 eV range of our calculation. For this purpose, the f -sum rule can be written:

$$N_{\alpha\alpha}^i = \frac{\Omega/a_0^3}{8\pi^2 E_0^2} \int_0^{h\nu_{max}} h\nu Im(\epsilon_{\alpha\alpha}(h\nu)) dh\nu, \quad (2)$$

where Ω denotes the unit cell volume, a_0 denotes the Bohr radius, and E_0 denotes the Rydberg energy. The value of $N_{\alpha\alpha}^i$ calculated from this formula should correspond to the number of initial state electrons per unit cell which are involved in optical excitation. We evaluated Eq. 2 and found $N_{\alpha\alpha}^i \approx 25$ for both polarizations and for both materials. Noting that there are 48 electrons per unit cell in the main portion of the valence band, associated with the O $2p$ orbitals, one would expect $N_{\alpha\alpha}^i$ to be approximately 48 when the oscillator strength is exhausted. In fact, within the 30 eV energy range which we studied, additional bound states, including Pb $6s$ and $5d$, Ca $3p$, and O $2s$ states, contributed to the imaginary part of the dielectric constant. This underestimate of $N_{\alpha\alpha}^i$ effects the real part of the dielectric constant that we evaluated using the truncated Kramers-Kronig transform. A very

simple argument based on form of the dielectric constant for a damped harmonic oscillator suggests that a reasonable correction to the Kramers-Kronig error is to add a positive constant to $Re(\epsilon_{\alpha\alpha}(h\nu))$ to account for the effects of higher energy transitions omitted from the integral. Unfortunately, the shape of the reflectivity curves is somewhat sensitive to this shift.

In order to compare our results with some recent reflectivity measurements [16], we shifted our calculated $Re(\epsilon_{aa}(h\nu))$ using the experimental value of the refractive index for $PbWO_4$ (2.25 at $h\nu = 1.9$ eV)[17]. Another well-documented error in our calculations is the underestimation of the band gap energy in density functional calculations.[13] Consequently, we also shifted our reflectivity curves along the $h\nu$ -axis by 1.2 eV. Our shifted reflectivity curves, assuming the electric field to be polarized along the a-axis, are compared with experimental measurements (where we do not know the polarization) in Fig. 9.

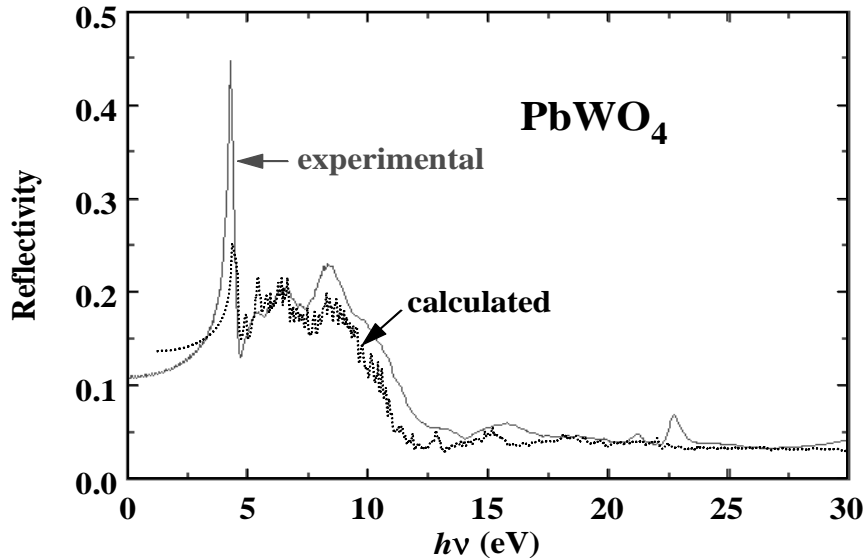


Figure 9: Comparison of the experimental reflectivity of Ref. ([16]) with calculated a-axis reflectivity, with a constant additional real part of the dielectric constant of 1.33 and shifted to higher energy by 1.2eV.

The agreement between the calculated and measured reflectivities shown in Fig. 9 is much greater than one would expect, given the various errors mentioned above and the inherent errors of the density functional approach. Ignoring the apologies for the moment, we see that the comparison of the calculated and measured reflectivity curves suggests that there reasonable correspondences in the shapes and magnitudes

of the two curves. The very sharp peak in the reflectivity near the band gap threshold has been interpreted as an excitonic effect.[16] However, our calculations show a similar sharp peak *without* including any excitons in the theory. In the theory, the sharp peak is due to the complicated band dispersions at the top of the valence bands and bottom of the conduction bands. We do not mean to suggest that excitons are not important in PbWO_4 , but possibly that their appearance in the reflectivity data is perhaps masked by a high density of band-to-band transitions near threshold.

Summary and conclusions

We have carried out self-consistent electronic structure calculations for several scheelite tungstate materials. In these calculations, the electronic density is variationally determined. We have analyzed that density in terms of molecular orbitals [7] which have been discussed throughout the literature. In addition to the important states associated with the tetrahedral WO_4 complex, we have identified some important contributions of the Pb 6s states, both to a narrow band below the main portion of the valence band and also to hybridization to states throughout the valence band.

We have calculated the imaginary part of the dielectric constant and have shown that, even within density functional theory, it is possible to show some similarity with existing experimental data for PbWO_4 . We have not yet attempted to make a similar comparison with older reflectivity measurements[18] for CaWO_4 .

In future work, we hope to consider the stability and electronic structure of various types of defects in these materials. The scintillation properties of these materials is of great interest, although it is more difficult to model with current computational tools.

Acknowledgments

This project was supported by NSF grants No. DMR-9403009, DMR-9706575, and DMR-9732023. We would like to thank A. Hofstaetter and A. K. S. Song for helpful discussions and Peter Blaha for help with the WIEN97 computer program.

References

- [1] W. Kohn and L. J. Sham, Physical Review **140**, A1133 (1965).
- [2] P. Hohenberg and W. Kohn, Physical Review **136**, B864 (1964).
- [3] Y. Zhang, N. A. W. Holzwarth, and R. T. Williams, Phys. Rev. B **57**, 12738 (1998).

- [4] P. Blaha, K. Schwarz, and J. Luitz, **WIEN97**, Vienna University of Technology, 1997. (Improved and updated Unix version of the original copyrighted WIEN-code, which was published by P. Blaha, K. Schwarz, P. Sorantin, and S. B. Trickey, in *Comput. Phys. Commun.* **59**, 399 (1990.)).
- [5] John P. Perdew and Yue Wang, *Phys. Rev. B* **45**, 13244 (1992).
- [6] Peter E. Blöchl, O. Jepsen, and O. K. Andersen, *Phys. Rev. B* **49**, 16223 (1994).
- [7] C. J. Ballhausen and Andrew D. Liehr, *Journal of Molecular Spectroscopy* **2**, 342 (1958).
- [8] G. Born, A. Hofstaetter, A. Scharmann, and B. Vitt, *Z. Physik B* **23**, 307 (1975).
- [9] G. Born, A. Hofstaetter, A. Scharmann, and B. Vitt, *Phys. Stat. Sol. (b)* **66**, 305 (1974).
- [10] G. Born, A. Hofstaetter, and A. Scharmann, *Z. Physik* **245**, 333 (1971).
- [11] G. Born, A. Hofstaetter, and A. Scharmann, *Phys. Stat. Sol. (b)* **37**, 255 (1970).
- [12] Robert M. Hazen, Larry W. Finger, and Joseph W. E. Mariathasan, *J. Phys. Chem. Solids* **46**, 253 (1985).
- [13] R. Del Sole and Raffaello Girlanda, *Physical Review B* **48**, 11789 (1993).
- [14] Michael Rohlfing and Steven G. Louie, *Physical Review Letters* **58**, 2312 (1998).
- [15] Robert Abt, Claudia Ambrosch-Draxl, and Peter Knoll, *Physica B* **194-195**, 1451 (1994).
- [16] I. A. Kamenskikh, V. N. Kolobanov, V. V. Mikhailin, I. N. Shpinkov, A. N. Vasil'ev, M. Kirm, and G. Zimmerer, Technical Report No. HASYLAB 1997 Annual Report, Part I, DESY Annual Report, Part I, 1997, p. 252-253.
- [17] G. F. Bakhshieva and A. M. Morozov, *Sov. J. Opt. Technol.* **44**, 542 (1977).
- [18] R. Grasser, E. Pitt, A. Scharmann, and G. Zimmerer, *Phys. Stat. Sol. (b)* **69**, 359 (1975).